Unsteady draining flows from a rectangular tank

Lawrence K. Forbes
School of Mathematics and Physics, University of Tasmania, Hobart 7001, Tasmania, Australia

Graeme C. Hocking
School of Mathematics and Statistics, Division of Science, Murdoch University, Murdoch 6150, Western Australia

(Received 15 November 2006; accepted 30 May 2007; published online 17 August 2007)

Two-dimensional, unsteady flow of a two-layer fluid in a tank is considered. Each fluid is inviscid and flows irrotationally. The lower, denser fluid flows with constant speed out through a drain hole of finite width in the bottom of the tank. The upper, lighter fluid is recharged at the top of the tank, with an input volume flux that matches the outward flux through the drain. As a result, the interface between the two fluids moves uniformly downwards, and is eventually withdrawn through the drain hole. However, waves are present at the interface, and they have a strong effect on the time at which the interface is first drawn into the drain. A linearized theory valid for small extraction rates is presented. Fully nonlinear, unsteady solutions are computed by means of a novel numerical technique based on Fourier series. For impulsive start of the drain, the nonlinear results are found to agree with the linearized theory initially, but the two theories differ markedly as the interface approaches the drain and nonlinear effects dominate. For wide drains, curvature singularities appear to form at the interface within finite time. © *2007 American Institute of Physics*.
[DOI: 10.1063/1.2759891]

I. INTRODUCTION

The study of the extraction of fluid from a reservoir has a long history. From a mathematical point of view, this free-surface flow can be regarded as one of the canonical nonlinear problems of fluid mechanics, as it has a particularly simple formulation. If the fluid is ideal, in the sense of being incompressible and flowing irrotationally, then its velocity potential satisfies Laplace's equation in the fluid, behaves like a mathematical sink near the extraction point, and obeys kinematic and dynamic boundary conditions at the free surface.

Much work has been done on the steady extraction of fluid. If the reservoir is of infinite depth and extraction occurs through a horizontal line sink, then the flow is effectively two-dimensional, and occurs in parallel vertical planes. From the work of Tuck and Vanden-Broeck,[1] Forbes and Hocking,[2] Hocking[3] and others it is now known that, for small extraction rates, the free surface forms a stagnation point directly above the sink, with small dips on either side. There is an upper value of the pumping rate beyond which steady solutions of this type no longer appear possible, and instead, some sort of unsteady flow is the only outcome. For somewhat larger pumping rates, there is evidently a critical value at which the free surface is drawn right down into the sink, so that the medium above the free surface is also entrained in the flow.

The situation for three-dimensional flow into an isolated point sink is somewhat similar. For low extraction rates, there is a steady solution which again has a stagnation point on the interface directly above the sink, and a small dip nearby that appears as an axially symmetric depression ring at the free surface. These steady solutions also have a limiting form at some maximum pumping rate, and in this case the physical mechanism is associated with the formation of a secondary circular ring of stagnation points on the interface. Details of these calculations are given by Forbes and Hocking.[4] Steady solutions to the more complicated situation in which a vertical reservoir wall is present near the extraction point have been computed by Forbes and Hocking.[5] It was again found that there was a maximum extraction rate beyond which steady solutions with surface stagnation points are evidently not possible.

Such results therefore focus attention on the behavior of fully unsteady solutions to the extraction problem. This is of considerable practical importance, since it indicates the interval of pumping extraction rates at which water can be withdrawn from the reservoir in a sustainable manner, without drawing the free surface into the sink.

Tyvand[6] considered unsteady flow due to a line source turned on impulsively, within a fluid of infinite depth. He performed a Taylor-series expansion in time, to third order, and used this approximate solution to estimate a critical withdrawal rate beyond which a dip would form at the interface and eventually accelerate into the sink. It is not clear to what extent such a low-order series expansion in time can predict such long-term behavior, but in any event the result is interesting, and predicts a lower value for the critical pumping rate than was obtained for purely steady solutions by Hocking and Forbes.[7] Tyvand[6] recognized that the starting conditions for the sink would doubtlessly influence the maximum pumping rate at which steady-state behavior could be achieved, and he anticipated that a slow and gradual sink turn on would most likely give rise to steady extraction at a rate closest to the theoretical maximum value.

The corresponding axisymmetric problem, in which the

unsteady withdrawal occurs through a point sink, was considered by Miloh and Tyvand.[8] They likewise performed a Taylor-series expansion in time, to the third order, and used this result to estimate the limiting pumping rate at which a dip forms at the free surface and the surface then collapses into the sink. Again, it is arguable the extent to which a low-order Taylor series can predict such long-term behavior, although good agreement with experimental results is evidently obtained.

Zhou and Graebel[9] modelled the draining of ideal fluid from a circular tank in which a circular hole of finite radius was centered on the bottom. The problem therefore possesses axially symmetric geometry. The flow was started impulsively and the results showed that, for a strong sink, a dip appears at the interface and is then drawn rapidly into the sink. However, when the sink is weaker, a reverse jet may appear at the interface, so that the central portion of the interface moves upward even as the interface is drawn down overall.

A similar analysis of an impulsively started point sink, although in an unbounded fluid, has been undertaken by Xue and Yue.[10] They found three different behavior types, determined by the Froude number (dimensionless sink strength). At low strength, the free surface possessed damped unsteady waves and evolved to a steady state configuration. For moderate Froude numbers, the interface was drawn down toward the sink but possessed an upwardly moving jet, and at high sink strengths the interface was drawn monotonically into the sink. These results are in accordance with those of Zhou and Graebel,[9] and similar findings have been made by Stokes, Hocking, and Forbes[11] for inviscid fluids, and by Baek and Chung[12] for an incompressible Newtonian viscous fluid.

It is interesting that the maximum Froude number at which Xue and Yue[10] could obtain steady solutions was much smaller than Froude numbers at which Forbes and Hocking[4] presented their steady results. This raises the question as to whether the Forbes and Hocking steady-state solutions are ever achievable in practice as the long-time limit of an unsteady calculation. On the other hand, it may also be the case that impulsively starting a flow from rest represents an extreme situation that precludes many steady-state flows from being attained; a more gentle method of turning on the sink may expand the range of Froude numbers for which steady flows are ultimately possible.

In the present paper, we likewise consider the impulsive start from rest of the flow in a tank, caused by a sink at the bottom. The problem is essentially the same as that studied by Farrow and Hocking,[13] although here we consider a tank containing two inviscid fluids flowing irrotationally and separated by a sharp interface. By contrast, Farrow and Hocking used a finite-difference technique to obtain solutions for the withdrawal of a viscous fluid with a continuously varying density profile that corresponded to an interface of some finite thickness. Their results showed that interfacial waves could be generated above the sink, then propagate outwards towards the edge of the tank, before being reflected at the walls and directed back inwards. These waves had a strong effect on the time at which the interface near the center of the tank would be drawn downwards into the sink. Those authors speculated that viscosity and interface thickness might have a smaller influence on the solution behavior than might be expected. The present paper examines this proposal, by investigating a system of two ideal fluids of different densities, separated by an interface of zero thickness.

The next section outlines the mathematical model of this draining tank situation, and presents a formulation for its solution. A linearized theory, valid effectively for small extraction rate through the sink, is discussed in Sec. III. The numerical scheme used to solve this problem is described in Sec. IV, and is based on a spectral representation of the velocity potential in each fluid layer. It therefore represents a generalization of techniques such as those presented by Dommermuth and Yue[14] and Kim *et al.*,[15] but makes use of some identities involving the time-dependent Fourier coefficients. This Fourier technique has recently been applied by Forbes, Chen, and Trenham[16] to the computation of a type of Rayleigh-Taylor instability, and permits overhanging interfaces to be calculated if they arise. Results are discussed in Sec. V, and it is found that unsteady waves formed on the interface have a strong influence on the details of how and when that interface is finally drawn into the sink. In some circumstances, it appears that Kelvin-Helmholtz-type instability may occur before final withdrawal. Some concluding remarks are given in Sec. VI.

II. MATHEMATICAL MODEL AND FORMULATION

We consider a rectangular tank in which a Cartesian coordinate system has been located with the x-axis lying horizontally along the bottom and the y-axis pointing vertically up the middle. The tank has width $2W$, so that its two walls are located at $x=-W$ and $x=W$. On the bottom of the tank is a hole of width $2A$, and we consider it to be placed symmetrically, so that it lies in the interval $-A<x<A$ on $y=0$.

Two fluids are present in the tank, and the interface between them initially lies on the horizontal line $y=H$. The lower and upper fluids have constant densities ρ_1 and ρ_2, respectively, following the notation in Batchelor (Ref. 17, p. 69), and since the lower fluid is the heavier, it follows that $\rho_1>\rho_2$. The top of the tank is located at height $y=H+L$. The acceleration of gravity is g, and is directed downwards.

The sink on the bottom is turned on abruptly at time $t=0$, and for simplicity it is assumed that a uniform outflow speed occurs over the sink $-A<x<A$. Fluid is withdrawn with mass flux $2Q$ (per width), which means that the fluid speed at the sink is $Q/(\rho_1 A)$. By continuity, the upper fluid must be recharged at the same volume flux across the top of the tank at $y=H+L$. Again, it is assumed for simplicity that the fluid there is injected uniformly, so that its downward speed is $Q/(\rho_1 W)$.

The interface between the two fluids is initially located at $y=H$, and as time progresses, it clearly must move downward under the influence of the sink at $y=0$ and the fluid recharge at $y=H+L$. The location of the interface is denoted by $y=\eta(x,t)$. If it remained horizontal, then it would simply be the case that $\eta(x,t)=H-(Qt)/(\rho_1 W)$ until at time

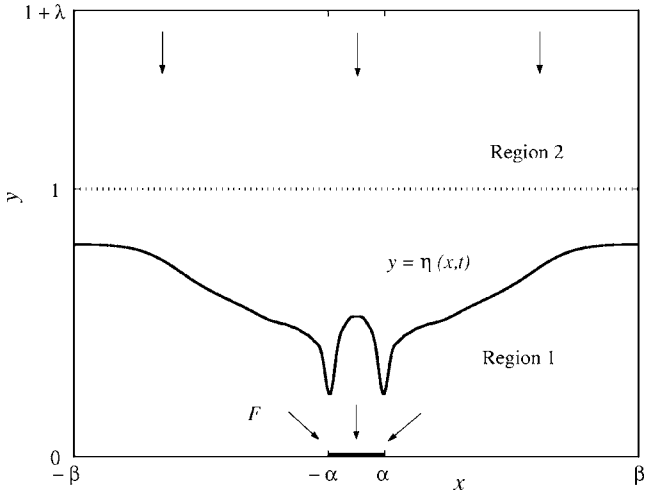

FIG. 1. Definition sketch of the two-fluid system in the tank, in dimensionless coordinates. The drain and the tank have half-widths α and β, respectively, and the total tank height is $1+\lambda$. The interface has been computed at time $t=77.3$ for a tank with $\alpha=2$, $\beta=20$, $\lambda=2/3$. The density ratio is $D=0.9$ and the Froude number is $F=0.1$. (The surface-tension parameter is $\sigma=0.01$.)

$t=\rho_1 WH/Q$ it would reach the bottom of the tank and drainage would be complete. However, the interface does not remain horizontal but develops travelling waves that have a strong influence on both the time and the nature of the flow when the interface reaches the drain.

It is convenient now to scale the problem, so that all the variables are represented in dimensionless form. The initial depth H of lower fluid 1 is chosen as the length scale and time is referred to as $\sqrt{H/g}$. With this choice, the natural speed scale is $\sqrt{gH}$. It is evident that the problem therefore depends on the five dimensionless constant parameters

$$\lambda = L/H, \quad \alpha = A/H, \quad \beta = W/H,$$
$$D = \frac{\rho_2}{\rho_1}, \quad F = \frac{Q}{\rho_1 H\sqrt{gH}}. \tag{2.1}$$

Thus, in these nondimensional variables, the initial interface height is 1 and the tank has total depth $1+\lambda$. The width of the tank is 2β and the hole in the bottom has width 2α. The density ratio between the two fluids is D, and it is assumed here that $D<1$. The final parameter F in the system (2.1) is a Froude number based on the initial depth of lower fluid 1. It is effectively a dimensionless measure of the pumping rate at the sink.

A sketch of the nondimensionalized flow situation is presented in Fig. 1, and is taken from an actual solution. The initial interface location is sketched with a horizontal dashed line at $y=1$. The location of a drain on the tank bottom is indicated, and arrows at the top of the diagram represent the constant recharge through the top of the tank, to compensate for the effect of the sink. The interface $y=\eta(x,t)$ is drawn with a heavier solid line.

Since each fluid is assumed to flow irrotationally, then the velocity vector in each may be expressed as the gradient of a velocity potential, in the form $u_k\mathbf{i}+v_k\mathbf{j}=\nabla\phi_k$, $k=1,2$. Here, u and v refer to velocity components in the x and y directions. Each fluid is incompressible, and therefore

$$\nabla^2\phi_1 = 0 \quad \text{in } 0<y<\eta(x,t) \tag{2.2a}$$

and

$$\nabla^2\phi_2 = 0 \quad \text{in } \eta(x,t)<y<1+\lambda. \tag{2.2b}$$

As there is no outflow through the sides of the tank, it follows that the conditions

$$u_1 = 0 \quad \text{on } x=\pm\beta, \quad 0<y<\eta,$$
$$u_2 = 0 \quad \text{on } x=\pm\beta, \quad \eta<y<1+\lambda \tag{2.3}$$

must apply there. The similar condition on the tank bottom, although taking into account the presence of the drain hole, gives

$$v_1 = \begin{cases} 0 & \text{if } \alpha<|x|<\beta \\ -F/\alpha & \text{if } |x|<\alpha \end{cases} \tag{2.4}$$

on $y=0$. At the top of the tank, the assumption of uniform recharge yields the condition

$$v_2 = -F/\beta \quad \text{on } y=1+\lambda. \tag{2.5}$$

Finally, it is necessary to specify conditions on the moving interface itself. Neither fluid is free to cross this surface, so that the two kinematic conditions

$$v_k = \frac{\partial\eta}{\partial t} + u_k\frac{\partial\eta}{\partial x} \quad \text{on } y=\eta \tag{2.6}$$

must be imposed at the interface for each fluid, $k=1,2$. There is also a dynamic condition, which stipulates that the fluid pressure must be continuous across the interface. An unsteady Bernoulli equation holds separately in each fluid (see Batchelor,[17] p. 387), from which the pressure in each layer can be calculated. Equating the two at the interface then gives the dynamic condition in the form

$$D\frac{\partial\phi_2}{\partial t} - \frac{\partial\phi_1}{\partial t} + \frac{1}{2}D(u_2^2+v_2^2) - \frac{1}{2}(u_1^2+v_1^2) + (D-1)\eta$$
$$= \frac{1}{2}(D-1)F^2/\beta^2 + (D-1)(1-(F/\beta)t) \quad \text{on } y=\eta. \tag{2.7}$$

Conservation of mass in each fluid layer leads to an auxiliary condition

$$\int_{-\beta}^{\beta}\frac{\partial\eta}{\partial t}dx = -2F \tag{2.8}$$

at the interface.

It is necessary to subtract a steady component $\phi^S(x,y)$ from each of the velocity potentials in Eqs. (2.2a) and (2.2b), in order for the Fourier series (used in Sec. IV) to converge. This function satisfies Laplace's Eqs. (2.2a) and (2.2b) in the entire tank $|x|<\beta$, $0<y<1+\lambda$, the side conditions (2.3) in the form $\partial\phi^S/\partial x=0$ on $x=\pm\beta$ and the top condition (2.5) written as $\partial\phi^S/\partial y=-F/\beta$ on $y=1+\lambda$. This function is easily seen to have the form

$$\phi^S(x,y) = -\frac{F}{\beta}y + \sum_{n=1}^{\infty} P_n^S \cosh\left(\frac{n\pi}{\beta}(1+\lambda-y)\right)\cos\left(\frac{n\pi x}{\beta}\right), \tag{2.9a}$$

with coefficients given by the expression

$$P_n^S = -\frac{\int_{-\beta}^{\beta} v_1(x,0)\cos(n\pi x/\beta)dx}{n\pi \sinh(n\pi(1+\lambda)/\beta)}. \tag{2.9b}$$

The quantity $v_1(x,0)$ in the integrand in Eq. (2.9b) is the vertical velocity component over the bottom of the tank. For the uniform outflow function given by Eq. (2.4), these coefficients become

$$P_n^S = \frac{2\beta F \sin(n\pi\alpha/\beta)}{n^2\pi^2\alpha \sinh(n\pi(1+\lambda)/\beta)}.$$

The velocity potentials are now expressed as

$$\phi_1(x,y,t) = \phi^S(x,y) + \Phi_1(x,y,t),$$
$$\phi_2(x,y,t) = \phi^S(x,y) + \Phi_2(x,y,t), \tag{2.10}$$

and the governing Eqs. (2.2)—(2.8) are rewritten in terms of the new reduced potentials Φ_1 and Φ_2. These clearly still satisfy Laplace's equations (2.2a), (2.2b), and the side conditions (2.3). However, the bottom condition (2.4) now becomes simply

$$\partial\Phi_1/\partial y = 0 \quad \text{on } y = 0 \tag{2.11}$$

and the top condition (2.5) similarly transforms to

$$\partial\Phi_2/\partial y = 0 \quad \text{on } y = 1+\lambda. \tag{2.12}$$

The auxiliary condition (2.8) is unchanged, and the new forms of the kinematic conditions (2.6) and the dynamic condition (2.7) at the interface are obtained in a straightforward way, after substitution of Eqs. (2.10) into these expressions.

A solution of this problem therefore consists of finding the time-dependent interface shape function $\eta(x,t)$ and the two reduced velocity potentials $\Phi_1(x,y,t)$ and $\Phi_2(x,y,t)$. The problem is highly nonlinear, and can therefore only be solved numerically. However, a linearized solution is possible, and is presented in the next section.

III. THE LINEARIZED SOLUTION

A linearized solution can be developed for small Froude number F, corresponding to weak extraction rate at the sink on the bottom. This solution is presented here, and follows a similar derivation to that in Farrow and Hocking.[13] It is necessary first to assume that the vertical velocity component across the bottom of the tank can be expressed as

$$v_1(x,0) = FV_{11}(x). \tag{3.1}$$

Similarly, the steady velocity potential in Eqs. (2.9a) and (2.9b) must be able to be written

$$\phi^S(x,y) = F\phi_1^S(x,y). \tag{3.2}$$

These forms (3.1) and (3.2) are clearly available for the outflow function (2.4).

The reduced potentials are expressed as perturbation expansions in powers of the Froude number F. We assume that

$$\Phi_1(x,y,t) = F\Phi_{11}(x,y,t) + \mathcal{O}(F^2),$$
$$\Phi_2(x,y,t) = F\Phi_{21}(x,y,t) + \mathcal{O}(F^2), \tag{3.3}$$

and that the interface elevation may be written

$$\eta(x,t) = 1 - (F/\beta)t + F\eta_1(x,t) + \mathcal{O}(F^2). \tag{3.4}$$

The linearized versions of Eqs. (2.2a) and (2.2b) for the first-order velocity potentials now become

$$\nabla^2\Phi_{11} = 0 \quad \text{in } 0 < y < 1 \tag{3.5a}$$

and

$$\nabla^2\Phi_{21} = 0 \quad \text{in } 1 < y < 1+\lambda. \tag{3.5b}$$

The function Φ_{11} satisfies the bottom condition (2.11), and Φ_{21} obeys the top condition (2.12). Both these functions satisfy the side conditions (2.3) in the form

$$\partial\Phi_{k1}/\partial x = 0 \quad \text{on } x = \pm\beta \qquad k = 1,2. \tag{3.6}$$

The kinematic conditions (2.6) with Eqs. (2.10) and (3.3) give the linearized relations

$$\frac{\partial\phi_1^S}{\partial y} + \frac{\partial\Phi_{k1}}{\partial y} = -\frac{1}{\beta} + \frac{\partial\eta_1}{\partial t} \quad \text{on } y = 1 \; k = 1,2, \tag{3.7}$$

where ϕ_1^S is the steady potential to first order in Froude number, as in Eq. (3.2). The dynamic condition (2.7) similarly linearizes to give

$$D\frac{\partial\Phi_{21}}{\partial t} - \frac{\partial\Phi_{11}}{\partial t} + (D-1)\eta_1 = 0 \quad \text{on } y = 1. \tag{3.8}$$

It is evident that the linearized reduced velocity potentials satisfying Eqs. (3.5a), (3.5b), and (3.6), with the additional conditions (2.11) and (2.12), must take the general forms

$$\Phi_{11}(x,y,t) = \sum_{n=1}^{\infty} P_{n1}(t)\cosh(n\pi y/\beta)\cos(n\pi x/\beta),$$
$$\Phi_{21}(x,y,t) = \sum_{n=1}^{\infty} R_{n1}(t)\cosh(n\pi(1+\lambda-y)/\beta)\cos(n\pi x/\beta), \tag{3.9}$$

and the first-order interface function must be

$$\eta_1(x,t) = \sum_{n=1}^{\infty} H_{n1}(t)\cos(n\pi x/\beta). \tag{3.10}$$

When (3.9) and (3.10) are substituted into the linearized kinematic conditions (3.7) and Fourier analyzed, the relationships

$$H'_{n1}(t) = (n\pi/\beta)[-P_{n1}^S \sinh(n\pi\lambda/\beta) + P_{n1}(t)\sinh(n\pi/\beta)],$$
$$H'_{n1}(t) = -(n\pi/\beta)[P_{n1}^S \sinh(n\pi\lambda/\beta) + R_{n1}(t)\sinh(n\pi\lambda/\beta)] \tag{3.11}$$

are obtained between the various Fourier coefficient func-

tions. Here, the (constant) coefficients in Eq. (2.9b) have been written in the first-order form $P_n^S = FP_{n1}^S$. The linearized dynamic condition (3.8) gives the additional set of equations

$$DR'_{n1}(t)\cosh(n\pi\lambda/\beta) - P'_{n1}(t)\cosh(n\pi/\beta) + (D-1)H_{n1}(t) = 0. \tag{3.12}$$

The three sets of Eqs. (3.11) and (3.12) may be combined to give the single set of differential equations

$$\frac{d^2H_{n1}(t)}{dt^2} + \frac{(1-D)}{\Gamma_n}H_{n1}(t) = 0 \tag{3.13}$$

for the coefficients of the interface function in (3.10), at each order. The constants Γ_n in (3.13) are defined to be

$$\Gamma_n = \frac{D\coth(n\pi\lambda/\beta) + \coth(n\pi/\beta)}{(n\pi/\beta)}. \tag{3.14}$$

The initial conditions appropriate to an impulsive start of the sink are

$$H_{n1}(0) = 0 \quad P_{n1}(0) = 0$$

and the differential Eq. (3.13), with conditions (3.11) and (3.12), yields the solution

$$H_{n1}(t) = -\frac{P_{n1}^S(n\pi/\beta)\sinh(n\pi\lambda/\beta)}{\sqrt{(1-D)/\Gamma_n}}\sin(t\sqrt{(1-D)/\Gamma_n}). \tag{3.15}$$

For the case of constant outflow through the sink, as given in Eq. (2.4), the linearized solution (3.15) may be written explicitly as

$$\eta(x,t) = 1 - \frac{F}{\beta}t - 2F\sum_{n=1}^{\infty}\frac{\sinh(n\pi\lambda/\beta)\sin(n\pi\alpha/\beta)\sin(t\sqrt{(1-D)/\Gamma_n})\cos(n\pi x/\beta)}{n\pi\alpha\sqrt{(1-D)/\Gamma_n}\sinh(n\pi(1+\lambda)/\beta)} + \mathcal{O}(F^2), \tag{3.16}$$

after use has been made of (2.9b), (3.4), and (3.10). The constant Γ_n is as defined in Eq. (3.14). Linearized solutions for the two velocity potentials have similar forms to (3.16), but these are not given here in the interests of brevity.

IV. THE NUMERICAL SOLUTION TECHNIQUE

In this section, we describe the numerical method used for the solution of the fully nonlinear system of equations developed in Sec. II. The technique is based on Fourier series to some order N for the two reduced velocity potentials Φ_1 and Φ_2 in Eq. (2.10) and the interface elevation η.

From Laplace's Eqs. (2.2a) and (2.2b) and boundary conditions (2.3), (2.11), and (2.12), the reduced velocity potentials have the approximate forms

$$\Phi_1(x,y,t) = P_0(t) + \sum_{n=1}^{N} P_n(t)\cosh(n\pi y/\beta)\cos(n\pi x/\beta),$$
$$\Phi_2(x,y,t) = R_0(t) + \sum_{n=1}^{N} R_n(t)\cosh(n\pi(1+\lambda-y)/\beta)\times\cos(n\pi x/\beta) \tag{4.1}$$

to order N. The linearized equivalent was given in Eq. (3.9). The two Fourier coefficients P_0 and R_0 in Eq. (4.1) are not actually needed in the final numerical solution, since only the spatial derivatives of velocity potentials are physically measurable as velocity components. We therefore set $R_0(t)=0$ in Eq. (4.1), but nevertheless solve for $P_0(t)$.

It is possible to express the interface shape function $\eta(x,t)$ directly as a Fourier series in x, similar to Eq. (4.1), and solve for the coefficients. We have done this, and the resulting method works well. However, a generalization of this technique is also available, which can accommodate overhanging portions in the interface profile. Both approaches were described in detail by Forbes, Chen, and Trenham.[16] Here, only the second, more general, approach will be presented.

To begin, the unsteady portion of each velocity component is defined in terms of spatial derivatives of Eq. (4.1). In lower fluid 1, we have

$$U_1(x,y,t) = \partial\Phi_1/\partial x = -\sum_{n=1}^{N}(n\pi/\beta)P_n(t)\cosh(n\pi y/\beta)\sin(n\pi x/\beta),$$
$$V_1(x,y,t) = \partial\Phi_1/\partial y = \sum_{n=1}^{N}(n\pi/\beta)P_n(t)\sinh(n\pi y/\beta)\cos(n\pi x/\beta) \tag{4.2}$$

and for upper fluid 2 we similarly obtain

$$U_2(x,y,t) = \partial\Phi_2/\partial x = -\sum_{n=1}^{N}(n\pi/\beta)R_n(t)\cosh(n\pi(1+\lambda-y)/\beta)\times\sin(n\pi x/\beta),$$
$$V_2(x,y,t) = \partial\Phi_2/\partial y = -\sum_{n=1}^{N}(n\pi/\beta)R_n(t)\sinh(n\pi(1+\lambda-y)/\beta)\times\cos(n\pi x/\beta). \tag{4.3}$$

It is also convenient to define steady velocity components, based on derivatives of the potential in Eq. (2.9a). These are denoted

$$u^S(x,y) = \partial\phi^S/\partial x = -\sum_{n=1}^{N} (n\pi/\beta) P_n^S \cosh(n\pi(1+\lambda-y)/\beta)\sin(n\pi x/\beta),$$
$$v^S(x,y) = \partial\phi^S/\partial y = -F/\beta - \sum_{n=1}^{N} (n\pi/\beta) P_n^S \sinh(n\pi(1+\lambda-y)/\beta) \times\cos(n\pi x/\beta), \tag{4.4}$$

where the constant coefficients P_n^S are given in Eq. (2.9b). These expressions (4.2)–(4.4) will be used extensively in the following, evaluated along the moving interface.

The numerical technique makes use of the Pythagorean arc length s along the interface, according to the usual relationship

$$ds^2 = dx^2 + d\eta^2. \tag{4.5}$$

As the flow is left-right symmetric, it is convenient to define $s=0$ at the point where the interface intersects the y-axis $x=0$, and to let $s=\pm L(t)$ at the two walls of the tank $x=\pm\beta$. This function $L(t)$ is unknown, and to be determined as part of the solution process.

Following Forbes, Chen, and Trenham,[16] we define a new arc length variable

$$\xi = \beta s/L(t) \tag{4.6}$$

which is now always confined to the known interval $-\beta < \xi < \beta$. In fact, $\xi=0$ at $x=0$ and $\xi=\pm\beta$ at $x=\pm\beta$. The interface location is now represented parametrically in terms of the new arc length variable (4.6) and time t by means of the expressions

$$x(\xi,t) = \xi + \sum_{n=1}^{N} A_n(t)\sin(n\pi\xi/\beta),$$
$$\eta(\xi,t) = 1 - (F/\beta)t + C_0(t) + \sum_{n=1}^{N} C_n(t)\cos(n\pi\xi/\beta). \tag{4.7}$$

In terms of this new variable ξ in Eq. (4.6), the arc length condition (4.5) becomes

$$\left(\frac{\partial x}{\partial \xi}\right)^2 + \left(\frac{\partial \eta}{\partial \xi}\right)^2 = \frac{L^2(t)}{\beta^2}. \tag{4.8}$$

The chain rule of calculus is used to recast derivatives of the interface elevation η, with respect to x and t in the kinematic and dynamic boundary conditions (2.6) and (2.7), as derivatives in terms of ξ and t in which the other variable is held constant. Thus we regard the interface elevation as a function of the form $\eta(x(\xi,t),t)$ and accordingly obtain

$$(\partial\eta/\partial x)_t = \frac{(\partial\eta/\partial\xi)_t}{(\partial x/\partial\xi)_t}. \tag{4.9}$$

The subscripts indicate the variables that are to be held constant in taking the partial derivatives. In addition,

$$(\partial\eta/\partial t)_x = (\partial\eta/\partial t)_\xi - \frac{(\partial\eta/\partial\xi)_t(\partial x/\partial t)_\xi}{(\partial x/\partial\xi)_t}. \tag{4.10}$$

These two relations (4.9) and (4.10) are substituted into the kinematic conditions (2.6). The first of these yields the equation

$$(v^S+V_1)\left(\frac{\partial x}{\partial\xi}\right)_t = \left(\frac{\partial\eta}{\partial t}\right)_\xi\left(\frac{\partial x}{\partial\xi}\right)_t - \left(\frac{\partial\eta}{\partial\xi}\right)_t\left(\frac{\partial x}{\partial t}\right)_\xi + (u^S+U_1) \times\left(\frac{\partial\eta}{\partial\xi}\right)_t \tag{4.11}$$

and a second relation may be derived by subtracting one kinematic condition in (2.6) from the other and using (4.9) and (4.10). The result is

$$[V_2 - V_1](\partial x/\partial\xi)_t = [U_2 - U_1](\partial\eta/\partial\xi)_t. \tag{4.12}$$

The dynamic condition (2.7) takes the form

$$D\frac{\partial\Phi_2}{\partial t} - \frac{\partial\Phi_1}{\partial t} + \frac{1}{2}D[(u^S+U_2)^2 + (v^S+V_2)^2] - \frac{1}{2}D[(u^S+U_1)^2 + (v^S+V_1)^2] + (D-1)\eta = \frac{1}{2}(D-1)F^2/\beta^2 + (D-1)(1-(F/\beta)t), \tag{4.13}$$

where the derivatives of Φ_1 and Φ_2 with respect to time t in (4.13) are still to be taken holding x and y constant (rather than the arc length coordinate ξ.)

The governing Eqs. (4.8) and (4.11)–(4.13) are now subjected to Fourier decomposition, with the aim of deriving a system of simultaneous nonlinear ordinary differential equations for the Fourier coefficients, which can be integrated numerically. The arc length condition (4.8) is first integrated over the interval $-\beta<\xi<\beta$, to obtain the zeroth Fourier coefficient. This yields an explicit formula for the half-length $L(t)$ of the moving interface, in terms of other coefficients. The result is

$$L^2(t) = \beta^2\left[1 + \frac{1}{2}\sum_{n=1}^{N}(n\pi/\beta)^2(A_n^2(t) + C_n^2(t))\right]. \tag{4.14}$$

The arc length condition (4.8) is now differentiated with respect to time t (holding ξ constant), to give

$$\frac{\partial x}{\partial\xi}\frac{\partial^2 x}{\partial t\partial\xi} + \frac{\partial\eta}{\partial\xi}\frac{\partial^2\eta}{\partial t\partial\xi} = \frac{L(t)L'(t)}{\beta^2} \tag{4.15}$$

and this relation (4.15) is Fourier decomposed by multiplying it by the basis functions $\cos(j\pi\xi/\beta)$, $j=1,\ldots,N$ and integrating over the interval $[-\beta,\beta]$. This eventually results in the expression

$$\sum_{n=1}^{N} (n\pi/\beta)\mathcal{M}_{jn}A_n'(t) - \sum_{n=1}^{N} (n\pi/\beta)\mathcal{N}_{jn}C_n'(t) = 0,$$
$$\text{for } j = 1, \ldots, N. \tag{4.16}$$

Here, it has been convenient to define the quantities

$$\mathcal{M}_{jn}(t) = \int_{-\beta}^{\beta} (\partial x/\partial\xi)\cos(n\pi\xi/\beta)\cos(j\pi\xi/\beta)d\xi,$$
$$\mathcal{N}_{jn}(t) = \int_{-\beta}^{\beta} (\partial \eta/\partial\xi)\sin(n\pi\xi/\beta)\cos(j\pi\xi/\beta)d\xi. \tag{4.17}$$

As each integrand in (4.17) is an even function of ξ, it is in fact only necessary to perform the integrals over $[0,\beta]$ by symmetry, and this gives an extra efficiency in the numerical solution technique.

Similar Fourier decomposition methods are applied to the first kinematic boundary condition (4.11) at the interface. The zeroth Fourier mode is first obtained simply by integrating the equation. Using integration by parts and the definitions (4.2) leads to the elegant identity

$$\int_{-\beta}^{\beta} (v^S + V_1)\frac{\partial x}{\partial\xi}d\xi = \int_{-\beta}^{\beta} (u^S + U_1)\frac{\partial \eta}{\partial\xi}d\xi - 2F.$$

This result is combined with the integration of the other terms in Eq. (4.11) to give

$$C_0(t) = -\frac{1}{2}\sum_{n=1}^{N} \frac{n\pi}{\beta}A_n(t)C_n(t), \tag{4.18}$$

after some algebra. A further result may be derived from this identity.

Theorem: The average interface height across the tank has the value

$$\eta_{\text{ave}}(t) = 1 - (F/\beta)t \tag{4.19}$$

that would be obtained if it simply remained horizontal.

Proof: The spatial average of the interface elevation is

$$\eta_{\text{ave}}(t) = \frac{1}{2\beta}\int_{-\beta}^{\beta} \eta(x,t)dx = \frac{1}{2\beta}\int_{-\beta}^{\beta} \eta(\xi,t)\frac{\partial x}{\partial\xi}d\xi.$$

The series expressions (4.7) are now substituted into this expression and the integrals evaluated using the orthogonality properties of the trigonometric functions. When the formula (4.18) is then employed, all the terms involving Fourier coefficients cancel exactly, leaving only the expression (4.19) for the average interface height as a function of time. This concludes the proof of the theorem.

The remaining Fourier modes in the first kinematic boundary condition (4.11) are obtained by multiplying by basis functions $\cos(j\pi\xi/\beta)$, $j=1,\ldots,N$ and integrating over $[-\beta,\beta]$, as done previously. After some algebra, this gives the result

$$\sum_{n=1}^{N} \left[\frac{1}{2}\beta(j\pi/\beta)(n\pi/\beta)A_j(t)C_n(t) + \mathcal{N}_{jn}\right]A_n'(t)$$
$$+ \sum_{n=1}^{N} \left[\frac{1}{2}\beta(j\pi/\beta)(n\pi/\beta)A_j(t)A_n(t) - \mathcal{M}_{jn}\right]C_n'(t)$$
$$= -(j\pi/\beta)\sum_{n=1}^{N} S_{jn}^{(1)}P_n(t) + (j\pi/\beta)\sum_{n=1}^{N} S_{jn}^{(2)}P_n^S$$
$$\text{for } j = 1, \ldots, N. \tag{4.20}$$

In this expression (4.20), the quantities $\mathcal{M}_{jn}$ and $\mathcal{N}_{jn}$ are as defined in Eq. (4.17). It has also proved convenient to define additional intermediate functions

$$S_{jn}^{(1)}(t) = \int_{-\beta}^{\beta} \sinh(n\pi\eta/\beta)\sin(n\pi x/\beta)\sin(j\pi\xi/\beta)d\xi,$$
$$S_{jn}^{(2)}(t) = \int_{-\beta}^{\beta} \sinh(n\pi(1+\lambda-\eta)/\beta)\sin(n\pi x/\beta)$$
$$\times\sin(j\pi\xi/\beta)d\xi. \tag{4.21}$$

The second kinematic interfacial condition (4.12) is likewise subjected to Fourier analysis as described above. Integration by parts shows that the zeroth Fourier mode is satisfied as an identity, and so yields no new information. The higher Fourier modes, obtained by multiplying by $\cos(j\pi\xi/\beta)$ and integrating as before, give the simple and elegant result

$$\sum_{n=1}^{N} [S_{jn}^{(1)}P_n(t) + S_{jn}^{(2)}R_n(t)] = 0 \quad \text{for } j = 1, \ldots, N \tag{4.22}$$

after integration by parts has been utilized. The two intermediate functions in this expression are as defined in Eq. (4.21).

It is convenient now to differentiate Eq. (4.22) and convert it into a system of ordinary differential equations, since it is easier to integrate an initial-value problem of this type, rather than to use (4.22) directly in a system of differential-algebraic equations. After some algebra, and making use of the Fourier series (4.2)–(4.4) and (4.7), along with the result (4.18), the differentiated version of Eq. (4.22) can be expressed in the final form

$$\sum_{n=1}^{N} [-K_{jn}A_n'(t) - L_{jn}C_n'(t) + S_{jn}^{(1)}P_n'(t) + S_{jn}^{(2)}R_n'(t)]$$
$$= (F/\beta)\int_{-\beta}^{\beta} (U_2 - U_1)\sin(j\pi\xi/\beta)d\xi \quad \text{for } j = 1, \ldots, N. \tag{4.23}$$

The intermediate functions $S_{jn}^{(1)}$ and $S_{jn}^{(2)}$ in Eq. (4.23) are as defined in (4.21), and we have also introduced the additional quantities

$$K_{jn}(t) = \int_{-\beta}^{\beta} \left[\frac{1}{2}(n\pi/\beta)C_n(t)(U_2 - U_1) + (V_2 - V_1) \times \sin(n\pi\xi/\beta) \right] \sin(j\pi\xi/\beta)d\xi,$$

$$L_{jn}(t) = \int_{-\beta}^{\beta} \left[\frac{1}{2}(n\pi/\beta)A_n(t) - \cos(n\pi\xi/\beta) \right] \times (U_2 - U_1)\sin(j\pi\xi/\beta)d\xi \tag{4.24}$$

for convenience of notation.

Finally, the dynamic boundary condition (4.13) is also subjected to Fourier analysis. The zeroth-order mode is again obtained by integrating (4.13), and results in a differential equation for the coefficient $P_0(t)$ in Eq. (4.1). [The other zeroth-order coefficient $R_0(t)$ is taken to be zero.] We obtain

$$-2\beta P_0'(t) + D\sum_{n=1}^{N} G_{0n}^{(2)} R_n'(t) - \sum_{n=1}^{N} G_{0n}^{(1)} P_n'(t) = -\frac{1}{2}DJ_0^{(2)} + \frac{1}{2}J_0^{(1)} + (D-1)(F^2/\beta - 2\beta C_0(t)). \tag{4.25}$$

The equations for the higher Fourier modes in Eq. (4.13) are derived as previously, and result in the expressions

$$D\sum_{n=1}^{N} G_{jn}^{(2)} R_n'(t) - \sum_{n=1}^{N} G_{jn}^{(1)} P_n'(t) = -\frac{1}{2}DJ_j^{(2)} + \frac{1}{2}J_j^{(1)} - \beta(D-1)C_j(t) \quad \text{for } j = 1, \ldots, N. \tag{4.26}$$

The intermediate functions appearing in Eqs. (4.25) and (4.26) are defined to be

$$G_{jn}^{(1)}(t) = \int_{-\beta}^{\beta} \cosh(n\pi\eta/\beta)\cos(n\pi x/\beta)\cos(j\pi\xi/\beta)d\xi,$$

$$G_{jn}^{(2)}(t) = \int_{-\beta}^{\beta} \cosh(n\pi(1+\lambda-\eta)/\beta)\cos(n\pi x/\beta) \times \cos(j\pi\xi/\beta)d\xi,$$

$$J_j^{(1)}(t) = \int_{-\beta}^{\beta} [(u^S + U_1)^2 + (v^S + V_1)^2]\cos(j\pi\xi/\beta)d\xi,$$

$$J_j^{(2)}(t) = \int_{-\beta}^{\beta} [(u^S + U_2)^2 + (v^S + V_2)^2]\cos(j\pi\xi/\beta)d\xi. \tag{4.27}$$

The integrands in Eqs. (4.21), (4.24), and (4.27) are all even, and so the integrations can be performed over only half the indicated domain, as with the quantities in (4.17). The auxiliary Eq. (2.8) may be shown to lead to the same conclusion as (4.18), and so adds no new information.

The system of $4N+1$ ordinary differential equations that derive from the arc length condition (4.16), the two kinematic conditions (4.20) and (4.23), and the dynamic conditions (4.25) and (4.26) are now integrated in time, using the standard fourth-order Runge-Kutta method in Atkinson (Ref. 18, p. 371). This requires a matrix equation to be solved for the Fourier coefficients at each time step in the method, but gives results of very high accuracy. The quadratures required for the evaluation of the intermediate functions (4.17), (4.21), (4.24), and (4.27) are carried out using the composite trapezoidal rule, which is exponentially accurate for periodic integrands. The total length $L(t)$ of the interface is then computed at each time step using Eq. (4.14). The initial conditions appropriate to the impulsive start of the sink at the bottom of the tank are simply that all the Fourier coefficients in Eqs. (4.1) and (4.7) are zero at time $t=0$.

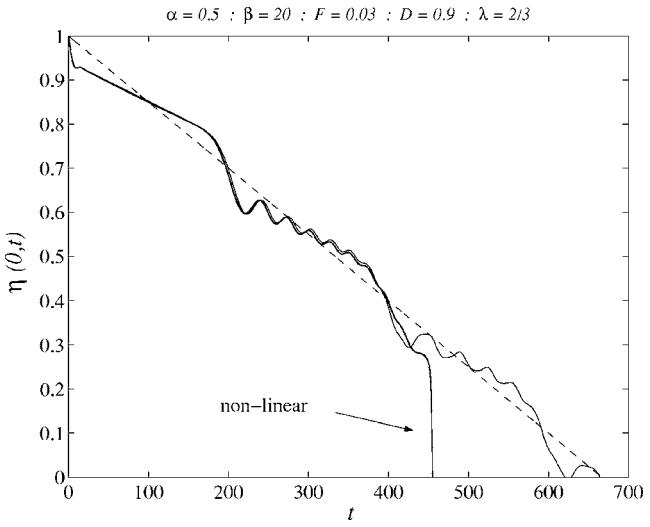

FIG. 2. Interface height at the center of the tank, as a function of time. The drain and tank half-widths are $\alpha=0.5$ and $\beta=20$. The Froude number, density ratio and initial upper-fluid depth are $F=0.03$, $D=0.9$, and $\lambda=2/3$, respectively. The average surface height (dashed line), linearized solution (thin line), and nonlinear interface location (heavier line, labelled) are shown.

V. PRESENTATION OF RESULTS

This solution algorithm was tested carefully by comparing the linearized solution of Sec. III with the fully nonlinear results computed using the algorithm in Sec. IV. It was confirmed that, for small times, the two results are in very good agreement. In addition, the results were checked, as far as possible, by comparison with the numerical solutions presented by Farrow and Hocking,[13] and in particular for their case number 15, which in the present notation requires $\alpha=5/12$, $\beta=20$, $\lambda=2/3$, $D=0.9$, and $F=0.0217$. Figures 3 and 4 in their paper were reproduced closely, in terms of the behavior of the surface that they identified as being equivalent to the interface in their continuously stratified model. This gives confidence in the predictions of the present approach, and incidentally confirms the Farrow and Hocking suggestion that viscosity and interface thickness may often play only a secondary role.

A solution computed with similar parameter values to the Farrow and Hocking test case is presented in Fig. 2. In this instance, the drain half-width is $\alpha=0.5$ (half the initial

depth of the lower fluid) and the Froude number is $F=0.03$. The remaining parameters are as above. In this diagram, the interface height $\eta(0,t)$ at the center of the tank, right above the drain, is shown as a function of time t. The straight dashed line represents the average interface height $\eta_{\text{ave}}(t)$ given in Eq. (4.19), and the thinner line is the result computed from the linearized solution (3.16). The heavier line is the nonlinear interface height (as indicated) evaluated at the center of the tank. It was computed with the algorithm in Sec. IV using $N=51$ Fourier coefficients, 201 spatial mesh points and 1601 time steps.

Clearly, there is close agreement between the linearized solution and the nonlinear computed result for $t<200$ and the agreement continues to be reasonable up until about $t=400$. Initially, the interface at $x=0$ draws down sharply, and in fact forms a dip above the drain. As time progresses, this dip widens, thus forming a travelling wave which progresses outwards from the center until it hits the tank walls at $x=\pm\beta$. The wave reflects from the walls with a 180° change of phase, and so moves back inward toward the center of the tank as a moving depression front. The arrival of that front at the center $x=0$ is clearly evident in Fig. 2, at about $t=200$. There is another phase change at the center, and the reflected wave then moves back outwards towards the tank walls. In its wake is a small train of wavelets, and these are evident in both the linearized and nonlinear solutions in Fig. 2, over the approximate time interval $230<t<360$. At about this time, nonlinear effects become important, and there is a marked deviation between the linearized and numerical results. A second reflected wave arrives back at the center of the tank at about $t=400$, and in the linearized solution, it undergoes yet another reflection and moves back outwards toward the tank walls. In the fully nonlinear solution, however, the wave front arriving at the tank center triggers an abrupt collapse of the interface into the sink, and this process is complete at about $t=460$.

In some numerical runs, it has been found that the interface profile develops small waves at about the time it collapses into the sink. These waves are numerical in origin, and are caused by an instability that appears in the method, close to the final stages of the flow. Decreasing the time step and grid spacing does not eliminate these waves, and increasing the number of Fourier coefficients reduces them only slightly, although at very greatly increased computational cost. It is likely that the numerical instability may be a reflection of a true physical instability at the interface, and this will be addressed again later.

To control these spurious waves, we have included an extra small surface tension effect in the dynamic condition. All that is required is to add a term $\sigma\kappa$ to the left-hand side of Eq. (2.7), in which σ is a dimensionless surface-tension parameter and

$$\kappa=\frac{\eta_{xx}}{[1+\eta_x^2]^{3/2}} \tag{5.1}$$

is the curvature of the interface. When written in terms of the arc length variable defined in Eq. (4.6), the curvature (5.1) becomes

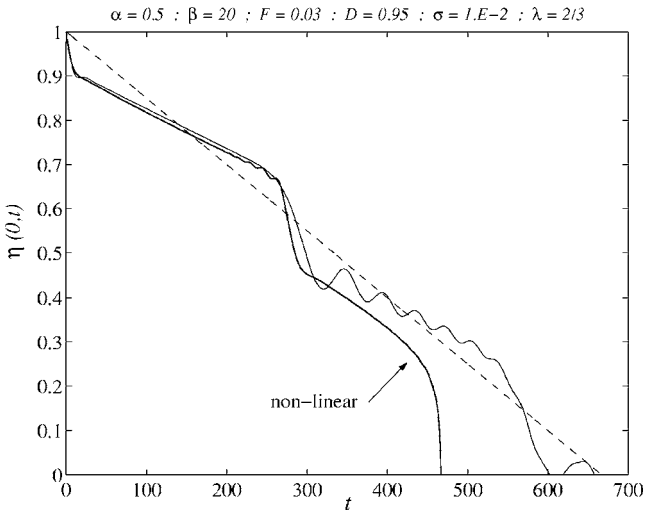

FIG. 3. Interface height at the center of the tank, as a function of time. The drain and tank half-widths are $\alpha=0.5$ and $\beta=20$. The Froude number, density ratio and initial upper-fluid depth are $F=0.03$, $D=0.95$, and $\lambda=2/3$, respectively. Surface-tension parameter $\sigma=0.01$ has been used. The average surface height (dashed line), linearized solution (thin line), and nonlinear interface location (heavier line, labelled) are shown.

$$\kappa=\frac{\beta^3}{L^3(t)}\left[\frac{\partial^2\eta}{\partial\xi^2}\frac{\partial x}{\partial\xi}-\frac{\partial\eta}{\partial\xi}\frac{\partial^2 x}{\partial\xi^2}\right]. \tag{5.2}$$

The function $L(t)$ in this expression (5.2) is the arc length along half the interface, and may be calculated from Eq. (4.14). The new dynamic condition at the interface, with this term added, must again be subjected to Fourier analysis and gives a modified form of conditions (4.25) and (4.26).

Figure 3 shows the behavior of the interface $\eta(0,t)$ at the center of the tank as a function of time, for a density ratio $D=0.95$. A small surface-tension parameter value $\sigma=10^{-2}$ has been utilized as the coefficient of the curvature κ in Eq. (5.2). Again, there is good agreement between the linearized and numerical nonlinear solutions for small times, and both show an abrupt dip in the interface elevation for early times and the effects of a reflected wave from the tank walls returning to the center. In the nonlinear solution, however, it is clear that this reflected wave triggers a collapse of the interface into the sink.

This behavior is evident in Fig. 4, where the interface profile has been plotted at six different times, to show the details of the withdrawal process. At $t=16$, a pronounced dip appears in the interface above the drain, but the rest of the interface remains horizontal although its mean level has dropped below its initial value 1. In the profile at $t=113$, it is evident that a travelling wave is moving outwards towards the tank walls. At the next time $t=209$, the wave has clearly reflected from the walls, with a 180° phase shift, and is moving back inwards toward the center. The waves have met at the tank center by time $t=306$, and although there is a further reflection that results in disturbances moving outward again, as for the linearized solution, it is also evident that this event triggers a rather sharp withdrawal of the interface towards the sink on the tank bottom. This occurs at about $t=466$. From Figs. 3 and 4, it is clear that nonlinear effects become important after about $t=300$.

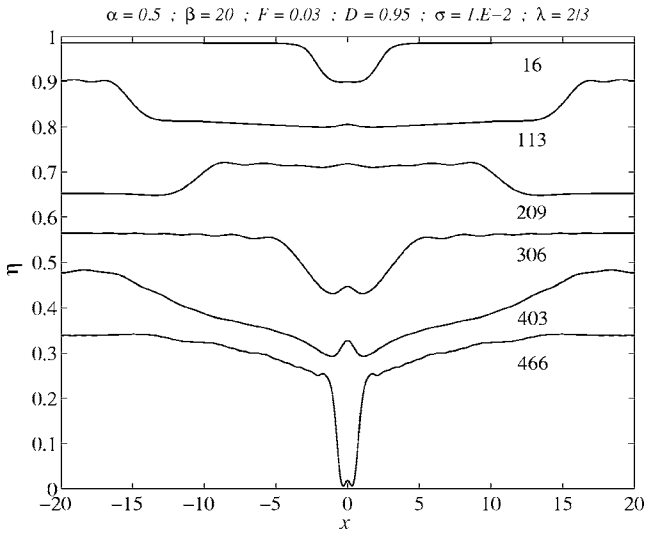

FIG. 4. A plot of interface shapes at six different times, for the same case as shown in Fig. 3.

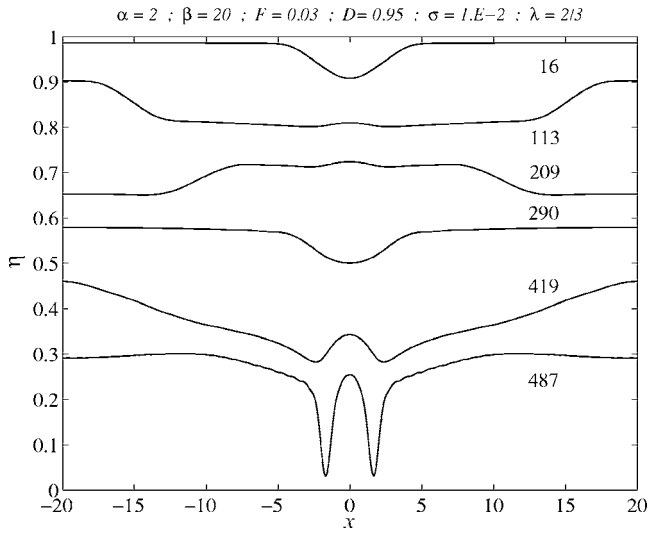

FIG. 6. A plot of interface shapes at six different times, for the same case as shown in Fig. 5.

Zhou and Graebel[9] observed that the nature of the flow near the time of final withdrawal was dependent upon the radius of the drain. For a narrow hole at the bottom of the tank, the interface was drawn smoothly down into the sink, but for a wider sink hole, it was possible for a reverse flow to occur, so that an upwardly moving jet formed at the center, even as the interface moved down overall.

This situation is investigated in Figs. 5 and 6. The Froude number and other parameters are unchanged from Figs. 3 and 4, except that, following Zhou and Graebel, the drain radius has been quadrupled to the new value $\alpha=2$. For small times, Fig. 5 gives a result rather similar to that shown in Fig. 3; there is an abrupt drop in the interface height at the center of the tank, and close agreement between the linearized and nonlinear solutions up until about $t=300$, when the

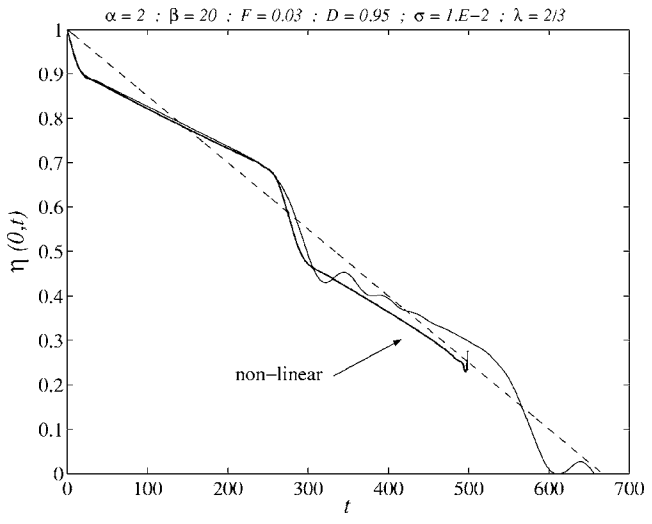

FIG. 5. Interface height at the center of the tank, as a function of time. The drain and tank half-widths are $\alpha=2$ and $\beta=20$. The Froude number, density ratio and initial upper-fluid depth are $F=0.03$, $D=0.95$, and $\lambda=2/3$, respectively. Surface-tension parameter $\sigma=0.01$ has been used. The average surface height (dashed line), linearized solution (thin line) and nonlinear interface location (heavier line, labelled) are shown.

reflected wave from the sides of the tank reaches back to the center. After about that time, nonlinear effects become important. However, in Fig. 5, the interface at the center of the tank moves rapidly *upwards* immediately before the solution method fails. This indicates the presence of an upwardly moving jet on the interface, at the center of the tank, consistently with the results of Zhou and Graebel.[9]

More details of this flow are visible from Fig. 6. As with Fig. 4, the flow starts with a pronounced dip on the interface near the center of the tank, and travelling waves then move outwards toward the tank walls. The waves are reflected with a change of phase and move back in towards the tank center when, in the nonlinear solution, they trigger a collapse of the interface into the sink. In Fig. 6 for the wider drain radius, however, there is clearly an upward moving jet at the center, even as the edges of this jet are pulled downwards into the sink. Stokes, Hocking, and Forbes[11] also observed this behavior in their investigations of unsteady flow into a line sink.

The question arises as to whether the dips either side of the central jet region are actually pulled into the sink, in some sense cutting off the jet from the rest of the lower layer of fluid, or whether some other situation occurs. It is, of course, difficult to answer such a question on the basis of numerical solutions alone, but an examination of the curvature of the interface suggests that another mechanism related to an actual physical instability may be taking place instead.

Figure 7(a) shows the curvature of the interface, computed from Eq. (5.2), for the same case as in Fig. 6, and for the early time $t=16$ and a later time $t=456$ close to the time at which the numerical method fails. It is found that the curvature κ possesses a rather unremarkable shape over much of the evolution of the interface, except close to the time at which the upward jet forms and the sides of the jet are pulled down. Then the curvature rapidly develops two large spikes, with maxima at the bottom of the two downwardly pointing cusps either side of the jet. We suggest that this behavior is evidence of Kelvin-Helmholtz instability,

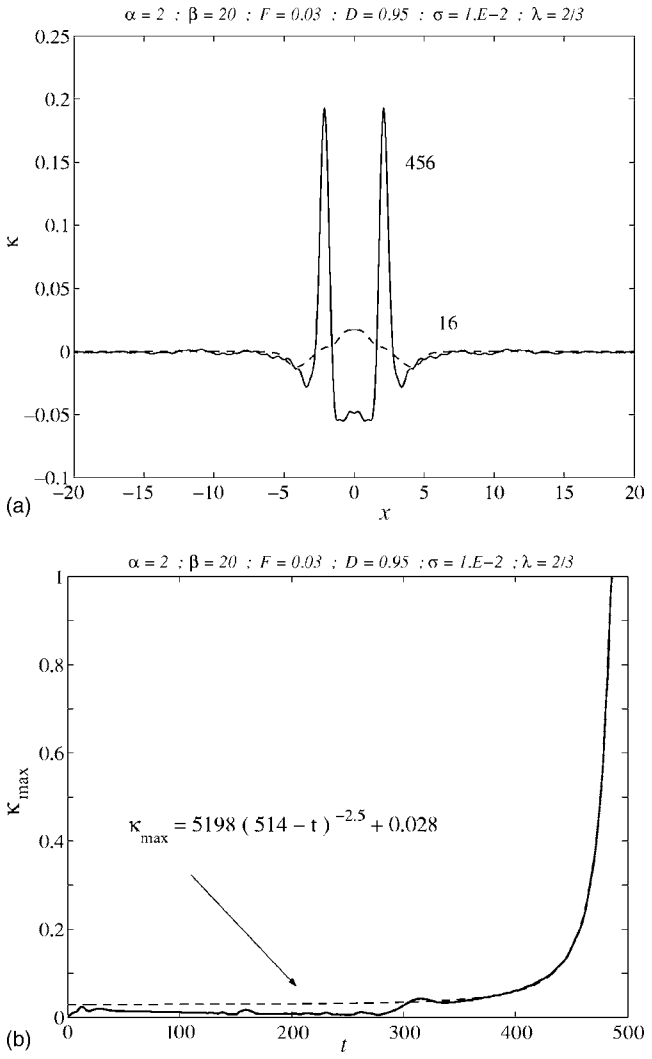

FIG. 7. (a) A plot of curvature κ at the interface for the same case as shown in Figs. 5 and 6, and for two different times; (b) plot of maximum curvature along the interface as a function of time, for the same case. The nonlinear results of the computation are shown with a solid line and the dashed line is the result of a power-law fit to these data for $t>350$.

which may occur in a stably layered fluid when one layer is in motion relative to another (see Chandrasekhar[19]). In particular, Moore[20] showed that the curvature must develop a singularity within finite time, and gave an estimate of this critical time for the situation in which an interface starts as a sinusoidal disturbance. At the critical time at which the Moore curvature singularity forms, the interface itself would possess a corner or a cusp, and models based on inviscid fluid mechanics would necessarily fail for later times. Later work by Krasny[21] and Baker and Pham[22] gives strong evidence that, if the interface is diffused over a finite region rather than being assumed to be infinitesimally thin, the formation of a singularity at the Moore critical time is avoided, and for later times the interface rolls up to form spiral billows. It is possible that some of the structures reported by Stokes, Hocking, and Forbes[11] may be associated precisely with the formation of spiral waves related to the Kelvin-Helmholtz instability.

For certain steady-state withdrawal flows, Cohen and Nagel,[23] Cohen,[24] and Courrech du Pont and Eggers[25] have found relatively simple scaling-law behavior between the curvature of the interface near the tip of a spike and its height above the withdrawing boundary. The unsteady flow studied in the present paper clearly represents more complex (and time-dependent) geometry for the interface than in those experimental studies, but we have nevertheless attempted to find similar scaling principles here, too. Figure 7(b) shows the result of such a study for the case discussed in Figs. 5 and 6. The solid line shows the growth of the maximum value of curvature along the interface, computed from Eq. (5.2), as a function of time t. For $t>350$, this maximum curvature is associated with the development of the downward spikes either side of the central jet near the drain hole, as illustrated in Fig. 6. There is clearly a very rapid rise in curvature at these points for $t>350$, and this is evident in Fig. 7(a).

Following Refs. 23–25, we have attempted to fit various functions to the solid curve in Fig. 7(b) for $t>350$, and have found that a close match is obtained with power laws of the form

$$\kappa_{\max} = a(t_0 - t)^b + c. \tag{5.3}$$

Nonlinear least-squares fitting (using a Nelder-Mead method) then gave $a \approx 5198$ and $c \approx 0.028$, with an exponent $b \approx -2.5$ and finite-time singularity formation in the curvature at $t_0 \approx 514$. This power-law curve (5.3) is drawn with a dashed line in Fig. 7(b), and gives strong support to the suggestion that finite-time curvature singularity does indeed occur at a time slightly later than that at which the numerical method fails.

Following Courrech du Pont and Eggers,[25] we have also computed the surface elevation at the downward spikes on the interface, and attempted to find a scaling law between it and the curvature at that point [plotted against time in Fig. 7(b)]. The best fits are again obtained with power laws similar to Eq. (5.3). However, unlike the steady-state case studied experimentally in Ref. 25, it is not possible in the present unsteady problem to find a good fit with the computed data. We conclude, therefore, that there is no reliable simple scaling law between interface height and curvature here. This is perhaps to be expected, since unlike the situation in Ref. 25, the interface here does not retain a simple cone shape above the withdrawal hole, but rather is influenced strongly by nonlinear travelling waves, as in Fig. 6, for example.

When the density ratio D between the upper and lower fluids approaches 1, the waves at the interface become larger. In that case, nonlinear effects become important earlier. An example of this is given in Fig. 8, where the interface height $\eta(0,t)$ at the center of the tank is shown as a function of time, for density ratio $D=0.99$ and the same value of the Froude number $F=0.03$ used previously. The drain half-width is $\alpha=0.5$. The linearized and nonlinear solutions both record a very significant drop in the interface height at early times, associated with the impulsive start of the sink, and although both then continue to drop monotonically, the nonlinear result decreases far more quickly, finally entering the sink at about time $t=324$.

The change of interface shape over time for this case is documented in Fig. 9. Profiles are shown for four different

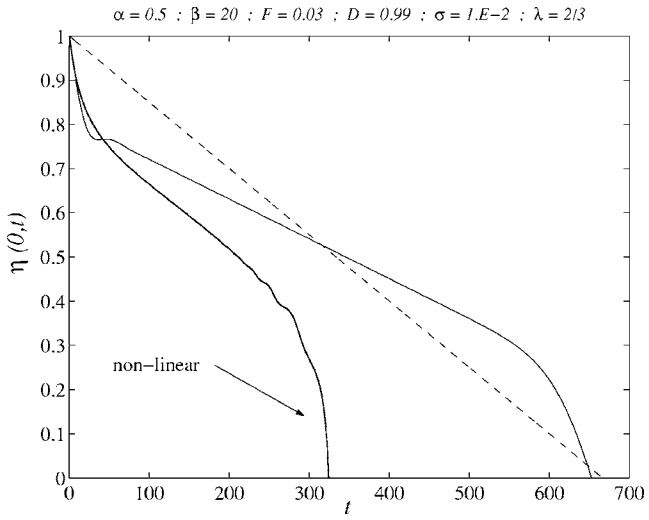

FIG. 8. Interface height at the center of the tank, as a function of time. The drain and tank half-widths are $\alpha=0.5$ and $\beta=20$. The Froude number, density ratio, and initial upper-fluid depth are $F=0.03$, $D=0.99$, and $\lambda=2/3$, respectively. Surface-tension parameter $\sigma=0.01$ has been used. The average surface height (dashed line), linearized solution (thin line) and nonlinear interface location (heavier line, labelled) are shown.

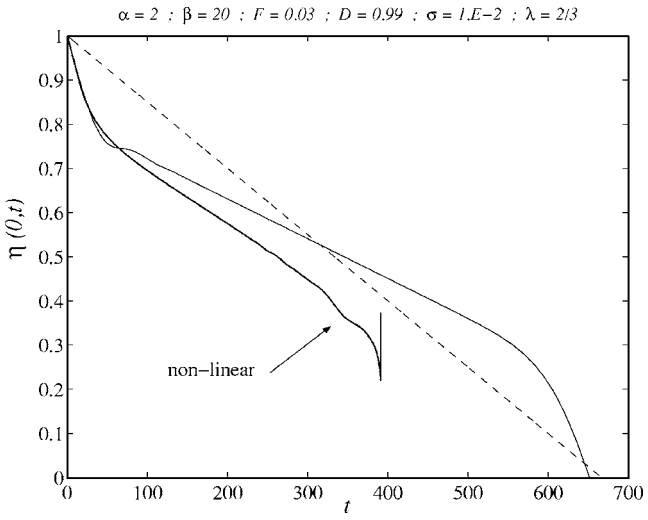

FIG. 10. Interface height at the center of the tank, as a function of time. The drain and tank half-widths are $\alpha=2$ and $\beta=20$. The Froude number, density ratio, and initial upper-fluid depth are $F=0.03$, $D=0.99$, and $\lambda=2/3$, respectively. Surface-tension parameter $\sigma=0.01$ has been used. The average surface height (dashed line), linearized solution (thin line) and nonlinear interface location (heavier line, labelled) are shown.

times. For the early time $t=16$ it is evident that a pronounced dip has occurred at the center of the interface while the remainder is horizontal. Outwardly moving waves are visible in the two later profiles at times $t=81$ and $t=193$, but these are not sufficient to interfere with the strong development of a downwardly moving jet that is drawn into the sink. The last profile at time $t=324$ gives a dramatic glimpse of the interface right at the time it enters the sink and the solution ceases.

As a further comparison with the results of Zhou and Graebel,[9] the effect of increasing the drain width for this density ratio $D=0.99$ are investigated in Figs. 10 and 11. In these diagrams, the drain half-width is $\alpha=2$. Figure 10 shows that there is good agreement between the linearized and nonlinear solutions in the early stages of the flow when a deep dip is formed on the portion of the interface above the drain, but that the nonlinear interface draws more rapidly toward the bottom than its linearized counterpart. However it ultimately forms an upwardly moving jet at the center of the tank, as with Fig. 5.

Further details of the flow are available from Fig. 11, where it can be seen that a strong dip first forms at the center of the tank, and travelling waves then move outward. The central portion of the interface moves downward strongly, but ultimately develops an upwardly directed jet, which can be seen in the last three profiles at times $t=274$, 306, and 370. Once again, the interface forms sharp dips either side of the upward jet, and it is possible that a Moore curvature singularity may form in finite time at these points, so preventing the solution from existing at later times.

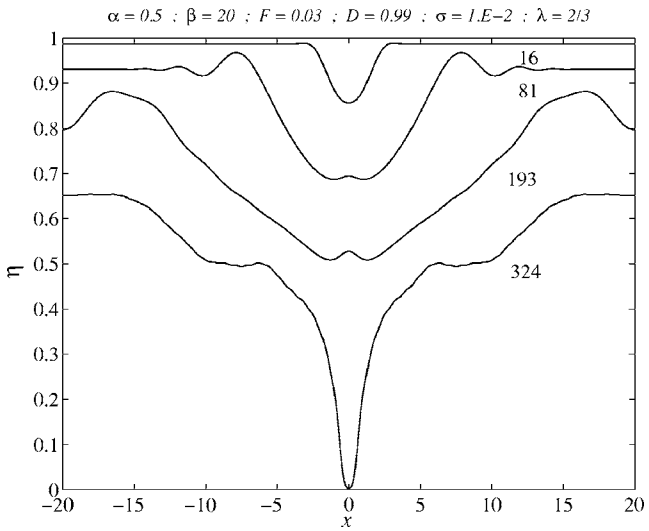

FIG. 9. A plot of interface shapes at four different times, for the same case as shown in Fig. 8.

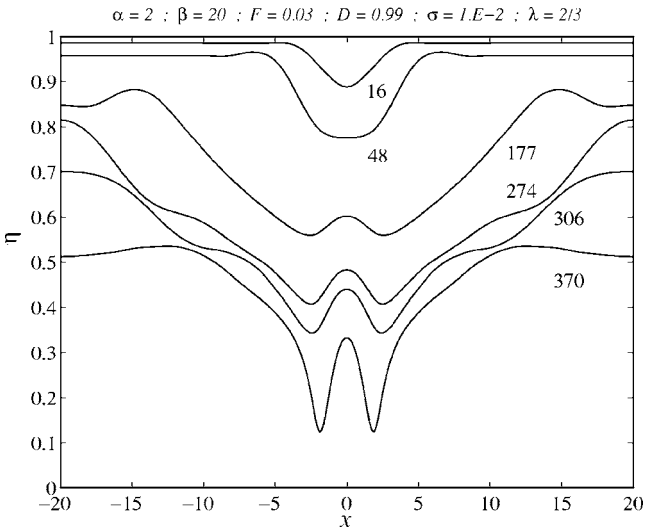

FIG. 11. A plot of interface shapes at six different times, for the same case as shown in Fig. 10.

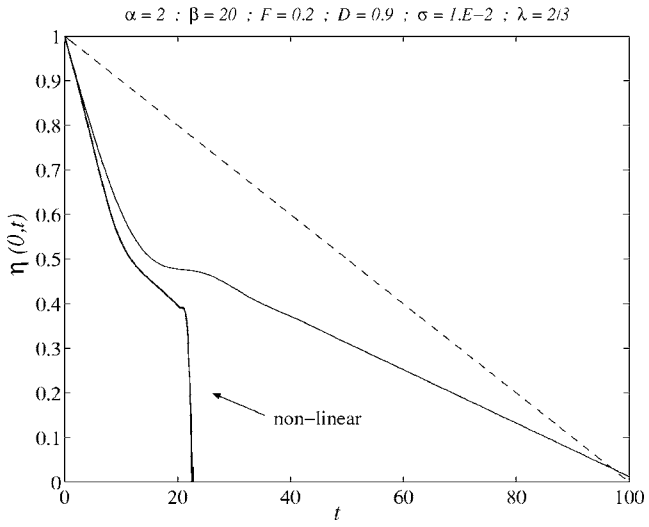

FIG. 12. Interface height at the center of the tank, as a function of time. The drain and tank half-widths are $\alpha=2$ and $\beta=20$. The Froude number, density ratio, and initial upper-fluid depth are $F=0.2$, $D=0.9$, and $\lambda=2/3$, respectively. Surface-tension parameter $\sigma=0.01$ has been used. The average surface height (dashed line), linearized solution (thin line), and nonlinear interface location (heavier line, labelled) are shown.

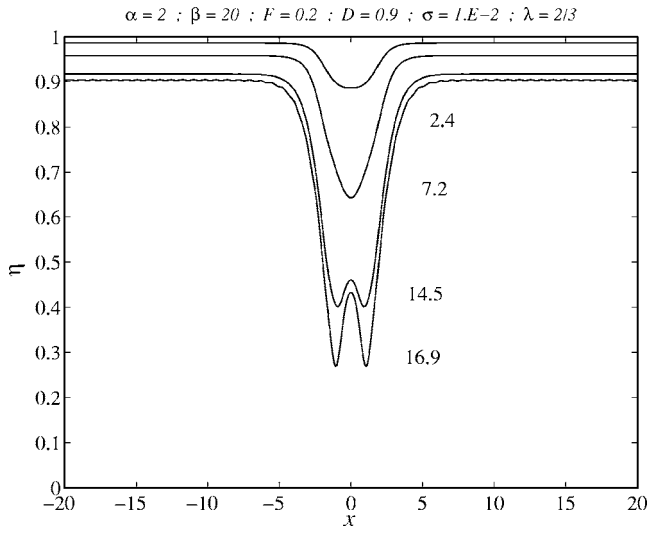

FIG. 13. A plot of interface shapes at four different times, for the same case as shown in Fig. 12.

We conclude this presentation of results with a brief investigation of the effect of increasing the Froude number F. It is to be expected from Sec. III that the linearized solution will become unreliable at earlier times, for larger Froude numbers, and Fig. 12 confirms that this is indeed the case. Here, the Froude number has been increased to $F=0.2$, which is about seven times those considered previously. Both the linearized and the nonlinear results indicate that the interface at the center of the tank is drawn downward very rapidly until about time $t=20$, and although the linearized interface height $\eta(0,t)$ at the center then slows its decrease while travelling waves move outward, the nonlinear elevation at the center continues to drop. A sudden instability in the nonlinear results appears at about $t=20$, making the results unreliable beyond that time, and this accounts for the very dramatic drop in interface height in Fig. 12.

Figure 13 shows four interface profiles for this case, and demonstrates the effect that the increased Froude number has upon the behavior. Unlike the situation in Fig. 4 for example, in which there was time for travelling waves to affect the interface shape, it is clear from Fig. 13 that there are apparently no such waves on the interface in the present case, and consequently the interface remains essentially flat except above the sink where it draws down rapidly. A reverse, upward facing jet eventually forms at the center, associated with the fact that the drain half width has the large value $\alpha=2$. The last time shown in Fig. 13 is the case $t=16.9$, when it is evident that there are deep dips that form either side of the upward facing jet, as before. For slightly later times than shown here, it is seen that these two dips move downwards very rapidly toward the tank bottom, and this appears to account for an instability that develops in the results at later times. This causes small wavelets on the interface to grow and the numerical solution then fails, and this is consistent with an instability, in which higher Fourier modes grow more rapidly. These small waves may be visible on the horizontal portions of the profile for the last solution shown in Fig. 13.

VI. DISCUSSION AND CONCLUSION

In this paper, solutions have been computed for the unsteady draining flow of a two-layer fluid in a rectangular tank. The flow is assumed to be two-dimensional, and the two fluids are ideal. As the heavier lower fluid is removed through the drain hole at the bottom, it is replaced at the top of the tank with an inflow of the upper lighter fluid entering at the same volume rate. Thus the sharp interface between the two fluids moves uniformly downward, and its average height has been shown to decrease linearly with time. Eventually, it reaches the sink at the bottom of the tank, and the model ceases to be valid.

For small Froude number, a linearized solution gives a reasonably good description of the flow over much of the time for which the model is valid. The impulsive start of the sink causes a dip to form on the interface above the drain, and this then develops into travelling waves that move outward towards the tank walls. There, they reflect back in towards the tank center, and do so with a change of phase. Eventually, the tank drains to an extent that the interface is close enough to the sink that nonlinear effects begin to dominate, and the linearized solution ceases to be accurate. This may be exacerbated by the travelling waves at the interface, and the details of how the interface is then drawn into the sink may depend on where the travelling wave fronts are, relative to the sink.

The nonlinear solutions have been computed using a somewhat novel spectral method proposed by Forbes, Chen, and Trenham.[16] It is essentially a straightforward Fourier-series type technique that derives from a representation of the solutions to Laplace's equations for the velocity potentials in the two fluid layers, but it makes use of some elegant identities to obtain a system of ordinary differential equations for the Fourier coefficients. These are solved using a Runge-Kutta approach to integrate them forward in time.

A wide range of solutions has been computed for different Froude numbers, drain widths, and density ratio D between the two fluids. When $D=0$ it has been found that the travelling waves on the interface are of small amplitude and move rapidly, so that there are many reflected waves produced between the tank walls and the center, before final withdrawal occurs. As $D\to 1$, however, the travelling waves move more slowly and have greater amplitude. This is as predicted by the linearized solution (3.16). Consistently with the work of Zhou and Graebel,[9] it has been found that the nature of the withdrawal process may be affected by the drain width. For narrow sink holes, the interface forms a downwardly directed jet which eventually reaches the bottom, but wider drains may produce a small *upwardly* directed jet above the drain. Zhou and Graebel suggested that the Rayleigh-Taylor flow instability (caused by a heavier fluid overlying a lighter one) may play a role in the final stages of the withdrawal process, but we have suggested this may be more likely to be a type of Kelvin-Helmholtz tangential shear instability at the interface. The sudden appearance of regions of very high curvature at the interface certainly suggests that an instability mechanism of some type is involved, and that singularity in the curvature is likely within finite time.

The results presented here for inviscid fluids separated by a sharp interface are at least qualitatively similar to those computed by Farrow and Hocking,[13] and appear to confirm their suggestion that interface thickness and viscosity may only have minor effects in some circumstances. A somewhat similar conclusion was obtained in the experimental studies of selective withdrawal from two fluids by Cohen and Nagel[23] and Cohen.[24] In those works, fluid was withdrawn from the upper layer, rather than the lower one as considered here. In addition, both fluids were effectively of unbounded extent, so that a steady-state flow was possible. It was found that the steady interface shapes followed certain scaling laws that were independent of the viscosity of the lower fluid. As the withdrawal rate from the upper fluid was increased, the curvature of the interface became very large, and eventually the lower fluid was withdrawn into the upper sink. Cohen *et al.*[26] suggest this may even be used as a technique for coating microparticles in industrial applications.

Although viscosity evidently has only a minor influence on these flows, it is nevertheless possible that the small amount of vorticity associated with viscous effects may permit spiral curl-up of the interface to be seen just before final withdrawal. This is particularly likely to occur with wide drains, for which an upwardly directed jet forms and regions of very high curvature develop at the interface. While such possibilities are fascinating from a theoretical point of view, they are nonetheless unlikely to have a major effect on the overall flow, and therefore may be expected to be of only limited interest to practical design engineers.

The spectral method presented here is capable of a generalization to a wide variety of different withdrawal scenarios. These will be discussed in future articles.

ACKNOWLEDGMENT

This research has been supported in part by Australian Research Council Grant No. DP0450225.

[1] E. O. Tuck and J.-M. Vanden-Broeck, "A cusp-like free-surface flow due to a submerged source or sink," J. Aust. Math. Soc. Ser. B, Appl. Math. **25**, 443 (1984).
[2] L. K. Forbes and G. C. Hocking, "Flow induced by a line sink in a quiescent fluid with surface-tension effects," J. Aust. Math. Soc. Ser. B, Appl. Math. **34**, 377 (1993).
[3] G. C. Hocking, "Supercritical withdrawal from a two-layer fluid through a line sink," J. Fluid Mech. **297**, 37 (1995).
[4] L. K. Forbes and G. C. Hocking, "Flow caused by a point sink in a fluid having a free surface," J. Aust. Math. Soc. Ser. B, Appl. Math. **32**, 231 (1990).
[5] L. K. Forbes and G. C. Hocking, "Flow due to a sink near a vertical wall, in infinitely deep fluid," Comput. Fluids **34**, 684 (2005).
[6] P. A. Tyvand, "Unsteady free-surface flow due to a line source," Phys. Fluids A **4**, 671 (1992).
[7] G. C. Hocking and L. K. Forbes, "A note on the flow induced by a line sink beneath a free surface," J. Aust. Math. Soc. Ser. B, Appl. Math. **32**, 251 (1991).
[8] T. Miloh and P. A. Tyvand, "Nonlinear transient free-surface flow and dip formation due to a point sink," Phys. Fluids A **5**, 1368 (1993).
[9] Q.-N. Zhou and W. P. Graebel, "Axisymmetric draining of a cylindrical tank with a free surface," J. Fluid Mech. **221**, 511 (1990).
[10] M. Xue and D. K. P. Yue, "Nonlinear free-surface flow due to an impulsively started submerged point sink," J. Fluid Mech. **364**, 325 (1998).
[11] T. E. Stokes, G. C. Hocking, and L. K. Forbes, "Unsteady free-surface flow induced by a line sink," J. Eng. Math. **47**, 137 (2003).
[12] J. H. Baek and H. Y. Chung, "Numerical analysis on axisymmetric draining from a cylindrical tank with a free surface," Comput. Fluid Dyn. J. **6**, 413 (1998).
[13] D. E. Farrow and G. C. Hocking, "A numerical model for withdrawal from a two-layer fluid," J. Fluid Mech. **549**, 141 (2006).
[14] D. G. Dommermuth and D. K. Yue, "A higher-order spectral method for the study of nonlinear gravity waves," J. Fluid Mech. **184**, 267 (1987).
[15] M.-J. Kim, H.-T. Moon, Y.-B. Lee, S.-K. Choi, Y.-K. Kim, H.-Y. Nam, and M. Cho, "A spectral method for free surface flows of inviscid fluid," Int. J. Numer. Methods Fluids **28**, 887 (1998).
[16] L. K. Forbes, M. J. Chen, and C. E. Trenham, "Computing unstable periodic waves at the interface of two inviscid fluids in uniform vertical flow," J. Comput. Phys. **221**, 269 (2007).
[17] G. K. Batchelor, *An Introduction to Fluid Dynamics* (Cambridge University Press, Cambridge, 1977).
[18] K. E. Atkinson, *An Introduction to Numerical Analysis* (Wiley, New York, 1978).
[19] S. Chandrasekhar, *Hydrodynamic and Hydromagnetic Stability* (Dover, New York, 1981).
[20] D. W. Moore, "The spontaneous appearance of a singularity in the shape of an evolving vortex sheet," Proc. R. Soc. London, Ser. A **365**, 105 (1979).
[21] R. Krasny, "Desingularization of periodic vortex sheet roll-up," J. Comput. Phys. **65**, 292 (1986).
[22] G. Baker and L. D. Pham, "A comparison of blob methods for vortex sheet roll-up," J. Fluid Mech. **547**, 297 (2006).
[23] I. Cohen and S. R. Nagel, "Scaling at the selective withdrawal transition through a tube suspended above the fluid surface," Phys. Rev. Lett. **88**, 074501 (2002).
[24] I. Cohen, "Scaling and transition structure dependence on the fluid viscosity ratio in the selective withdrawal transition," Phys. Rev. E **70**, 026302 (2004).
[25] S. Courrech du Pont and J. Eggers, "Sink flow deforms the interface between a viscous liquid and air into a tip singularity," Phys. Rev. Lett. **96**, 034501 (2006).
[26] I. Cohen, H. Li, J. L. Hougland, M. Mrksich, and S. R. Nagel, "Using selective withdrawal to coat microparticles," Science **292**, 265 (2001).